

Article

Dual-Frequency Retrieval of Soil Moisture from L- and S-Band Radar Data for Corn and Soybean

Tien-Hao Liao ^{1,*} and Seung-Bum Kim ²¹ Division of Geological and Planetary Sciences, California Institute of Technology, Pasadena, CA 91109, USA² Jet Propulsion Laboratory, California Institute of Technology, Pasadena, CA 91109, USA

* Correspondence: thaoliao@outlook.com

Abstract: Radar backscattering responds differently to soil moisture due to vegetation effects depending on the microwave frequency. The retrieval of soil moisture using a single frequency has been common. In this paper, we study how soil moisture retrieval performs using dual-frequency radar backscattering (L- and S-bands) compared with using L-band only. The dual-frequency inputs increase the amount of independent information, which is expected to reduce the uncertainty in estimating soil moisture. Forward scattering models for corn and soybean fields were previously generated and validated with the L-band for the SMAPVEX12 campaign: they are inverted as an independent test for the retrieval of soil moisture using the SMEX02 campaign data in this paper. It is demonstrated that L-band modeling of forward scattering processes is scalable at the S-band, in that the physics and parameters behind modeling the vegetation effects remain the same between L- and S-bands. Either L- or S-band single-frequency retrieval has reliable performance for soil moisture retrieval. Furthermore, averaging the retrieved soil moisture from both frequencies further improves the retrieval performance. The averaging avoids the determination of the weights of the L- and S-band σ_0 during the cost function minimization. The dual frequency retrieval is evaluated with the unbiased RMSE of 0.031 and 0.057 m^3/m^3 for corn and soybean, respectively, which are improvements by up to 0.010 and 0.004 m^3/m^3 , compared with single-frequency cases. The findings here can apply to the upcoming NISAR mission featuring L- and S-bands.

Keywords: dual-frequency; soil moisture; NISAR

Citation: Liao, T.-H.; Kim, S.-B. Dual-Frequency Retrieval of Soil Moisture from L- and S-Band Radar Data for Corn and Soybean. *Remote Sens.* **2022**, *14*, 5875. <https://doi.org/10.3390/rs14225875>

Academic Editors: Mehrez Zribi, Xiaojun Li, Hongliang Ma, Frédéric Frappart, Zanpin Xing and Nicolas Baghdadi

Received: 25 September 2022

Accepted: 16 November 2022

Published: 19 November 2022

Publisher's Note: MDPI stays neutral with regard to jurisdictional claims in published maps and institutional affiliations.



Copyright: © 2022 by the authors. Licensee MDPI, Basel, Switzerland. This article is an open access article distributed under the terms and conditions of the Creative Commons Attribution (CC BY) license (<https://creativecommons.org/licenses/by/4.0/>).

1. Introduction

Soil moisture is essential information for understanding the water cycle and related disasters. In recent years, algorithms using polarimetric synthetic aperture radar (PolSAR) to retrieve soil moisture have evolved rapidly [1,2]. NASA's Soil Moisture Active Passive (SMAP) mission [2] was launched in January 2015 utilizing L-band radar and radiometer to provide global soil moisture maps. The 3-month worth of radar data have been acquired and their inversion was validated to show the potential to monitor global soil moisture [3]. The upcoming NASA ISRO SAR (NISAR) mission featuring L- and S-bands will be launched in 2024, allowing for global soil moisture information [4]. NISAR will provide maps of surface soil moisture globally every 6 to 12 days at the spatial scale of 200 m. This could offer unprecedented details to monitor croplands and perform hazard management [5].

Various algorithms have been studied for soil moisture retrieval with a view toward global application. Change detection concepts assume temporally static roughness and/or vegetation [1,6]. The decomposition of fully polarimetric data allowed retrieval via surface components [7]. The physical model for scattering can be inverted with rigorous constraints [8]. There is also an inversion of the parametric forward model [9], machine learning [10,11], and statistical Bayesian estimation [12]. At the L-band, the physical modeling approach was expanded for global application by developing vegetation scattering models for different vegetation types. It was successful to apply the inversion of the physical model to estimate soil moisture for the same vegetation [13,14] in wider regions. The

physical models were validated against the airborne and field measurements, followed by inverting the models using the time-series radar data over grassland, croplands, and forest [14–18]. Globally, the SMAP active soil moisture products using the same approach were validated globally [3].

In this paper, we incorporate the S-band backscattering coefficient data into the retrieval algorithm that uses both L- and S-bands. The goal is to evaluate the potential of the dual-frequency inversion, primarily for applying to the NISAR observations. Although there are many studies of radiometer and radar synthesis for soil moisture retrieval [19], there are only very few studies of L- and S-band synthesis, due partly because of rare simultaneous observations. The airborne Passive and Active L- and S-Microwave Instrument (PALS) instrument was one of the few and collected L- and S-band measurements during the Soil Moisture Experiments in 2002 (SMEX02) [20] and the 1999 Southern Great Plains (SGP99) experiment [21]. Narayan et al. studied the retrieval of soil moisture from SMEX02 by employing linear or multiple regressions between the co-located radar backscatter and the in situ soil moisture dataset [22]. Similarly, Bolten applied a combination of multiple regression analyses for soil moisture retrieval using the SGP99 data [21]. Although both have utilized backscattering coefficients in the retrieval process, there was no specific analysis of the performance with L and S dual-frequency inputs.

The novelty of this paper is, first, that the forward physical models derived for corn and soybean fields using the SMAPVEX12 field campaign data [15,16] were successfully applied to the soil moisture retrieval for the independent data set from SMEX02. This success supports the prospect that the algorithm may apply in wider areas observed by satellite missions. Second, the time-series algorithm for dual-frequency provides improved soil moisture retrieval in terms of unbiased RMSE compared to that from the L-band input only. The algorithm is applied to dual frequencies, L- and S-band, in this paper. The definition of unbiased RMSE can be referred to in Equation (5) in our previous paper [23]. We also list them in Equation (4) in this paper.

This paper is organized as follows: Section 2 describes the SMEX02 field campaign. Section 3 presents the theory for the retrieval algorithm and the scattering method. Section 4 shows the results. Section 5 is a discussion of the results. Section 6 summarizes the conclusion.

2. SMEX02 Field Campaign

The SMEX02 (Soil Moisture Experiments in 2002) experiment in Walnut Creek Watershed, Iowa, was conducted from mid-June to mid-July in 2002. The primary focus of SMEX02 is to improve the understanding of the global water cycle, especially on soil moisture and its exchange with the atmosphere. The experiment aimed at the validation of soil moisture retrievals produced by PALS, 1.26 GHz at the L-band and 3.15 GHz at the S-band. The extent of PALS coverage is about 7 by 35 km².

The PALS flights were deployed on 8 days listed in Table 1, where backscattering coefficients (σ^0) were acquired. The incidence angle for the recorded lines is mostly within 43 to 45 degrees.

Table 1. Sampling dates of backscattering coefficients (σ^0), soil moisture (M_v), and vegetation water content (VWC); highlight for overlapping dates.

Data	Date (yr. 2002)
Backscattering coefficients (σ^0)	25 June, 27 June, 1 July, 2 July, 5 July, 6 July, 7 July, 8 July
Soil moisture (M_v)	25 June, 26 June, 27 June, 1 July, 5 July, 6 July, 7 July, 8 July, 9 July, 11 July, 12 July
Vegetation Water Content (VWC)	2 to 4 times during 15 June and 9 July (varying by sites)

During the campaign, in situ volumetric soil moisture (M_v) data were measured at corn and soybean fields [21]. The land cover for Walnut Creek was primarily agricultural with corn and soybeans being the dominant crops. Flight lines shown in Figure 1 were repeated for other flight days except for July 1, when there were only four lines in the

south. PALS acquired backscattering coefficients and brightness temperature at both L- and S-bands. The overlapping days of soil moisture sampling with PALS flights were the 25 and 27 of June and the 1, 5, 6, 7, and 8 of July, in total 7 days. Scattered thunderstorms during the experiment on 4 July and 6 July provide drying and wetting conditions for the analysis [24].

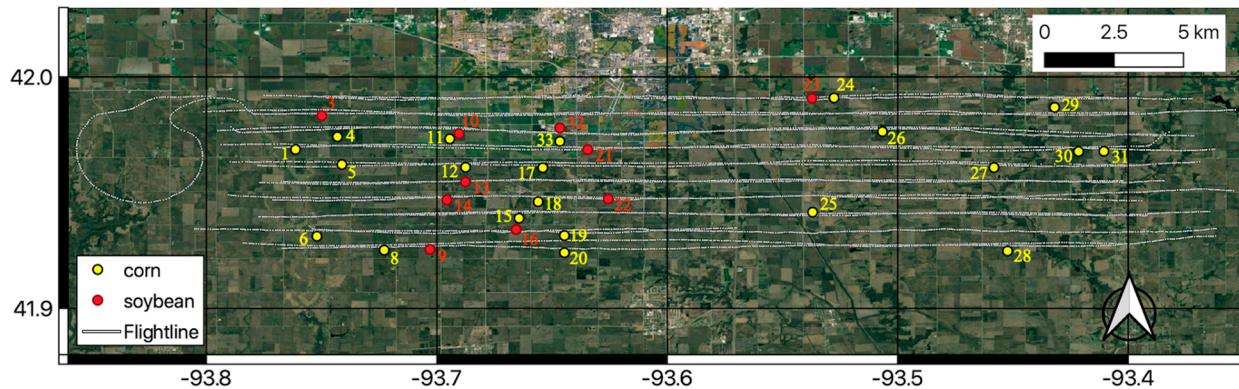


Figure 1. PALS flight lines on 25 June 2002, during SMEX02. There are 21 corn and 10 soybean fields. Site numbers are shown in numeric. It shows the location of recorded σ^0 and crop information for one day.

Vegetation sampling includes the destructive measurement of vegetation water content (VWC) and the crop structure [25]. Since the vegetation grew relatively slowly over time than soil moisture change, vegetation was sampled only two to four times between June 15 and July 9. During the periods of the PALS overflight, June 25 to July 8, there are mostly two to three times of vegetation sampling. However, we did observe an obvious increase in VWC during the flight period from these limited samplings. During the PALS flight period, the corn VWC ranged mostly between 3 and 5 kg/m² and the soybean VWC was less than 1 kg/m². To fill the dates when in-situ VWC values from destructive sampling were unavailable, while both σ^0 and M_v were observed, we used VWC derived from the normalized difference water index (NDWI) [26] as a VWC reference for the study. For the soil roughness, each site was characterized by one-time surface roughness sampling. The grid board photography method was used.

The interpolation was performed for both L- and S-band to assign σ^0 from recorded flight lines to the in situ soil moisture locations in Figure 1. The field numbers in Figure 1 are for either corn or soybean fields. For the corn and soybean fields in SMEX02, there were both plants grown perpendicular and parallel to the flight direction. We found there was no obvious relation between backscattering and row direction for both crops.

3. Forward Model for σ^0 and Soil Moisture Retrieval

The physical model here refers to the electromagnetic modeling of the vegetated surface [27–29]. The backscattering is calculated using a physical model and the backscatter varies with the geometry of vegetation, the roughness of the soil, and the dielectric property of both vegetation and soil. For soybean plants, we apply distorted Born approximation which is a single scattering model. For corn plants, with stronger scattering among plants, we apply a multiple scattering model.

The flow of the retrieval algorithm is summarized in Figure 2. The flow chart is shared for the analysis of corn fields and soybean fields in this paper. PALS provides measured backscattering coefficients in quad-polarizations, VV, HH, HV, and VH for both L- and S-bands. The ground parameters to be estimated include soil moisture, VWC, and surface roughness. The strategy we adopted is that we separated the σ^0 into co-polarization and cross-polarization. The L-band HV is used to estimate the first guess of VWC. The estimated VWC then serves as ancillary inputs for the retrieval. On the other hand, the co-polarization

data are inputs to the retrieval. The purpose of the separation is that co-polarization has better sensitivity for soil moisture while cross-polarization senses vegetation better. To establish the relationship between σ^0 and ground parameters, we apply forward models through precomputed lookup tables (LUT). The lookup table makes it convenient for rapid retrieval. Separate LUTs were computed for different vegetation covers. The cost function for co-polarized σ^0 was minimized in the least-square sense to retrieve soil moisture and surface roughness. In the end, the in situ and retrieved soil moisture were compared for validation. The modules of the algorithm in Figure 2 are further detailed in the following sections.

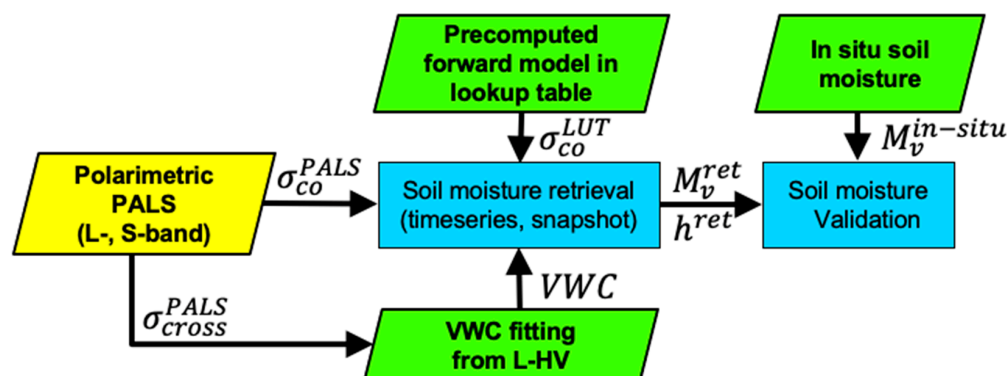


Figure 2. Soil moisture retrieval and validation flow chart. VWC stands for vegetation water content; LUT for lookup table.

3.1. Physical Model and Lookup Tables

Physical models are established by input parameters and the computation of scattering. The inputs include the shape and the size of the scatterers as well as the dielectric constant of the vegetation element. These geometric and dielectric properties are connected by allometric relation to (e.g., Equation (2) [14]) the amount of water inside the vegetation, VWC. The input parameters were measured during the SMAPVEX12 campaign [17]. With these inputs, physical scattering models allow the calculation of the backscattering coefficients from these scatterers.

A merit of the physical models is that they are not limited to empirical regression in a localized field campaign. For the same vegetation type, the electromagnetic scattering from the vegetation layer is widely applicable from Maxwell's equation perspective regardless of the location on the globe (as long as crop variety is not significant). This physical insight allows the model's validity to extend from the model's development sites. To test this concept of general applicability, we inverted the physical models established from the SMAPVEX12 field campaign in Winnipeg [15,16] to perform the soil moisture retrieval in SMEX02, a new independent location. In this paper, this model is used for inversion with the SMEX02 data on the following bases. The two campaigns share the same L-band frequency, justifying the L-band application to SMEX02. Since both frequencies, L- and S-, were acquired at the same time during SMEX02, the same vegetation parameters may apply to establish the physical models for both L- and S-band. Below is a brief description of previous studies of physical models on corn fields and soybean fields.

For corn plants, the multiple scattering model derived from the vector radiative transfer theory is chosen [16]. For vegetation such as corn, the stalk of the plant is much thicker than most crops such as soybean and wheat. This results in large albedo, meaning that the scattering is comparable to the absorption by the corn plant. These increased scattering energies among corn plants are included through a higher-order accounting as the multiple scattering effects. In the later stage of corn growth, the stalk is thick and tall. Multiple scattering effects are essential to increase the total backscattering coefficients: otherwise, the absorption becomes large with single scattering processes alone. These findings were numerically confirmed [16]. Specifically, the vegetation parameters include the structure of corn stalks and leaves as well as the volumetric moisture content of corn

plants. The generic volumetric moisture content from [30] is used to calculate the plant dielectric constant for corn and soybean plants at both L- and S-bands. For the corn plant, we modeled stalks using finite cylinders and leaves using disks. We used consistent physical parameters from the SMAPVEX12 field campaign in this study for SMEX02. Geometric observations in the SMAPVEX12 fields provided values of the geometry and density of scatterers. The values are available in Figure 4 and Table 3 in [16].

With the regard to the surface component of the corn scattering model, Numerical Maxwell Method 3D (NMM3D) was used at the L-band [31]. The existing L-band NMM3D does not cover the same rms height range at the S-band and, the Advanced Integral Equation Method (AIEM) [32] is used instead. We only use the co-polarized backscattering coefficients from AIEM as the physical model is inverted only using co-polarization. The surface scattering either from NMM3D at L-band or AIEM at S-band is further attenuated by the vegetation.

For soybean plants, the overall simulation strategy is the same as in the corn's case, by employing the vegetation parameter observations and the physical scattering model from the SMAPVEX12 campaign. Unlike the corn's case, multiple scattering is insignificant for small plants like soybean. We implemented the single scattering model based on the distorted Born approximation [27]. It is also referred to as an incoherent model. Huang et al. proposed a coherent model simulating the scattering from young soybean plants to solve the underestimation of backscattering coefficients by the incoherent model [15]. Compared to the incoherent model, the coherent model enhances the backscattering power when VWC is low especially for HH [15]. The major difference of up to 0.4 dB occurs when VWC is below 0.2 kg/m². For VWC above 0.2 kg/m², the difference is not significant. The field-by-field statistics of the difference is shown in Table III in [15]. While considering the physical model for the soybean field for SMEX02, there are very little data with VWC less than 0.2 kg/m². The incoherent model should achieve similar accuracy as that from the coherent model for SMEX02. The surface scattering simulation is the same as in the corn case: NMM3D for the L-band and AIEM for S-band. For the soybean plant we modeled stalks and stems using a finite cylinder and leaves using disks. Similar to corn, we used the same physical parameters as SMAPVEX12's in this study. The values for geometry and density of scatterers are available in Figure 5 and Table 2 in [15].

3.2. VWC Estimated from L-Band HV, as Input to Retrieval

VWC is an important input to the forward model inversion. The vegetation parameters discussed in the previous section evaluate VWC and are represented by VWC as one of the three axes of the LUT. During the inversion, VWC input slices the 3D-LUT, and the consequent 2-D LUT simplifies the search of the soil moisture and roughness solutions. VWC data can be obtained from the destructive samples of the SMEX02 fieldwork, which is the most accurate. However, for wider application, our strategy is to use a generalized relationship per crop using simultaneous radar observations of co- and cross-polarizations. As one of the generalized metrics, Kim and Van Zyl used radar vegetation index (RVI) defined as $RVI = 8\sigma_{hv} / (\sigma_{hh} + \sigma_{vv} + 2\sigma_{hv})$ [33]. It involves both co-polarized and cross-polarized backscattering coefficients. Ma et al. estimated VWC from the regression analysis using various combination of polarimetric data from SMEX02 [34]. Ma et al. concluded that the best estimation for corn's VWC was found using L-band co-polarized ratio $\sigma_{hh} / \sigma_{vv}$. For soybean, the best estimation for VWC was through L-band $\sigma_{hh} / \sigma_{hv}$. To examine general applicability of these, RVI and Ma et al.'s formulas were applied to the independent data, that is, SMAPVEX12 data. Both low and high VWC had the same RVI, which makes RVI ineffective when trying to estimate VWC as an input to soil moisture retrieval. When Ma et al.'s formula for corn was applied to the SMAPVEX12 data, the estimated VWC became negative. According to Ma et al.'s formula for soybean, VWC is inversely proportional to $\sigma_{hh} / \sigma_{hv}$ while SMAPVEX12 data show the opposite trend. This discrepancy may be caused by the selective use of the training data by Ma et al. Based on our Figure 1 and Table 1,

there should be five times more data for both corn and soybean from SMEX02 than used by Ma et al.

Facing the above discrepancies, in this paper, VWC was instead estimated from L-band HV using the regression formula derived using the SMAPVEX12 data. We found the regression relation between VWC and L-band HV in the dB scale. They were shown in Equations (1) and (2) without VWC_{adjust} . The SMAPVEX12 data offered the backscattering coefficients at multi-angles ranging from 30 to 50 degrees of incidence. There was no obvious difference in the regression result between the lower and higher incidence. Then we need only one regression formula for one crop. For the same crop in the SMEX02 campaign, we introduced an additional term VWC_{adjust} to Equations (1) and (2) to take into account the VWC bias among two different campaigns. Additionally, it ensures that there is no negative VWC estimated while deriving using SMEX02's L-band HV. In Section 4.1, we estimate the statistic error among the regression and VWC derived from the normalized difference water index (NDWI) for SMEX02 data. The latter one serves as a reference VWC. The formula for corn was based on 211 data while for soybean from 324 data. VWC_{adjust} were set to 1.0 kg/m² for corn and 0.06 kg/m² for soybean.

$$VWC_{corn} = 0.22\sigma_{HV}^{L-band} + 6.47 + VWC_{adjust} \quad (1)$$

$$VWC_{soybean} = 0.07\sigma_{HV}^{L-band} + 2.51 + VWC_{adjust} \quad (2)$$

In Sections 3.1 and 3.2 so far, we have described all the inputs needed for soil moisture retrieval.

3.3. Single-Frequency Time-Series Retrieval

The soil moisture retrieval algorithm uses the time-series input backscattering coefficient HH at one frequency. Only HH is considered so that the algorithm may apply to the NISAR's acquisitions (HH and HV are received in most cases). Equation (3) describes the cost function for N time-series data. This formula is applied to both the L- and S-band, respectively. The cost function is

$$cost^{TS} = \sum_{t=1}^N \left(\sigma_{HH}^{LUT}(h, \varepsilon_t, VWC_t) - \sigma_{HH,t}^{mea} \right)^2 \quad (3)$$

where TS denotes the time-series with N measurements. $\sigma_{HH,t}^{mea}$ stands for the measured HH and σ_{HH}^{LUT} stands for HH from the lookup table. h is rms height and it is assumed temporally static at each field.

As illustrated in Figure 3, first, lookup tables were generated at coarse intervals of soil moisture, roughness, and VWC. For the retrieval, we would like to search the lookup table with finer precision, so the lookup table is firstly interpolated to the finer intervals of the axis's variables. The HH varies smoothly with these variables, which justifies the interpolation. Then, each 2-D slice of the lookup table at each candidate estimate of the rms height is extracted and the cost associated with the rms height candidate is computed based on Equation (3) with the input from measured time-series HH. The minimum cost is determined to locate the retrieved RMS height and the retrieved time-series soil moisture.

For each RMS height, RMSi in Figure 3, Equation (3) is applied to compute the cost function. The time-series retrieval was validated globally using the SMAP radar data [35]. A key assumption of time-series retrieval is that the rms height h changes slowly and is held constant over the retrieval period. There are $N + 1$ unknowns to retrieve: N soil dielectric constant plus 1 rms height. The soil moisture and dielectric constant is interchangeable using the Mironov's dielectric formula [36]. Since there are N -observed HH in Equation (3), the estimation may be considered ill-conditioned, in that the number of knowns is smaller than the number of unknowns. The SMAP radar data acquired HH and VV, but NISAR will produce only HH over the majority of the world.

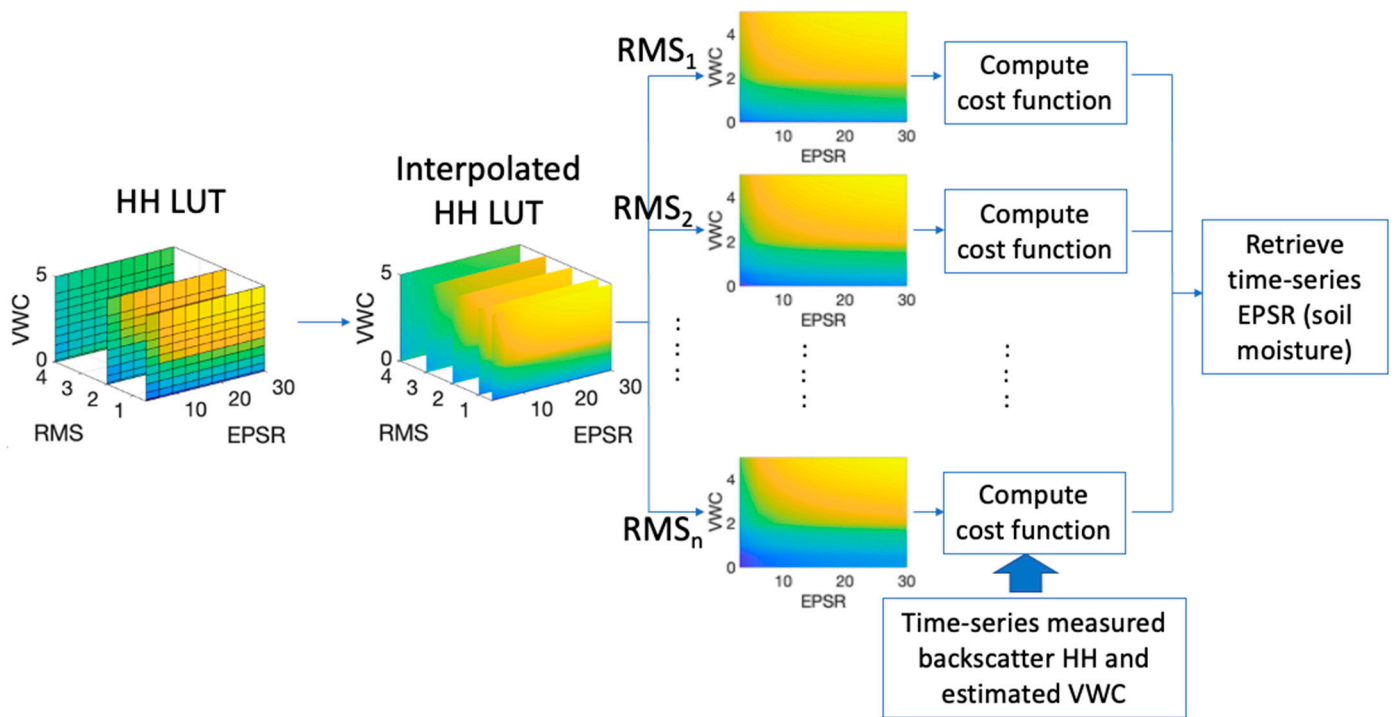


Figure 3. Time-series retrieval algorithm flow. RMS_i is a candidate of time-invariant estimate of roughness. EPSR stands for real part of dielectric constant. Unit for VWC and RMS are kg/m² and cm, respectively.

The error statistics metric used in this paper are as follows, especially root mean square error (RMSE) and unbiased RMSE (ubRMSE).

$$\begin{aligned}
 \Delta(t_n) &= \sigma_{model}^0(t_n) - \sigma_{observation}^0(t_n) \text{ or } m_{v,retrieval}(t_n) - m_{v,in\ situ}(t_n) \\
 bias &= \frac{\sum_{n=1}^N \Delta(t_n)}{N} \\
 rmse &= \sqrt{\frac{\sum_{n=1}^N (\Delta(t_n))^2}{N}} \\
 ubrmse &= \sqrt{\frac{\sum_{n=1}^N (\Delta(t_n) - bias)^2}{N}} = \sqrt{rmse^2 - bias^2}
 \end{aligned} \tag{4}$$

3.4. L- and S-Band Time-Series Retrieval

To resolve the ill condition of single-frequency retrieval, the feasibility of dual-frequency inputs is considered. Since the L- and S-band are two independent channels, there are few ways to combine their contribution for retrieval.

One way to implement the algorithm is by doubling the observables in the cost function with N observed L-HH and N observed S-HH backscattering. Then the summation term in Equation (3) will feature two squared terms instead of one, $(\sigma_{L-HH}^{LUT}(h, \epsilon_t, VWC_t) - \sigma_{L-HH,t}^{mea})^2$ and $(\sigma_{S-HH}^{LUT}(h, \epsilon_t, VWC_t) - \sigma_{S-HH,t}^{mea})^2$. We tried the retrieval with equal weighting of the two squared terms. Overall, the unbiased RMSE is 0.047 m³/m³ for corn and 0.060 m³/m³ for soybean with the statistics complied over all the fields. The performance is not better than single frequencies for both crops. A possible explanation is that the sensitivity of the backscatter difference in the cost function is not the same at the two frequencies. In forward comparison for corn, we observed that the dynamic range of measured backscatter over the time series is larger for the L-band than the S-band. Then adding the S-band to the cost function would not impact the search for the minimum cost significantly. In other words, an equal weighting between the L- and S-band's cost function is not sufficient to represent

the sensitivity. However, we have not experimented with the optimization of weighting coefficients at present.

An alternative way to incorporate the dual frequency for the retrieval is to combine them in the soil moisture domain. This includes two single-channel retrievals, L- and S-bands, respectively, using Equation (3) and the same retrieval flow in Figure 3. Each of the retrievals will finally give its time-series retrieved soil moisture. As mentioned in Section 3.3, the single channel retrieval is slightly underdetermined given $N + 1$ unknowns retrieved by N observables. We now average the retrieved soil moisture from L- and S-bands to obtain the final retrievals of soil moisture. Although each single frequency retrieval experiences a slightly under-determined inversion, the averaging of the results from the two independent channels may reduce the ill condition. We will demonstrate the improved results in the next section.

4. Results

4.1. VWC Estimation from L-HV

To prepare VWC from HV as an input to the retrieval, the regression-based coefficients derived from the SMAPVEX12 campaign were applied to the SMEX02 L-band HV (Equations (1) and (2)). Figure 4 shows that the regression of the HV-based VWC is in good agreement with the reference. The references were estimated using the normalized difference water index (NDWI) data on the dates of SMEX02 PALS flights [26]. Destructive VWC samples were collected mostly two to three times during the flight period. Due to the scarcity, NDWI-VWC was used a reference to compare with HV-VWC.

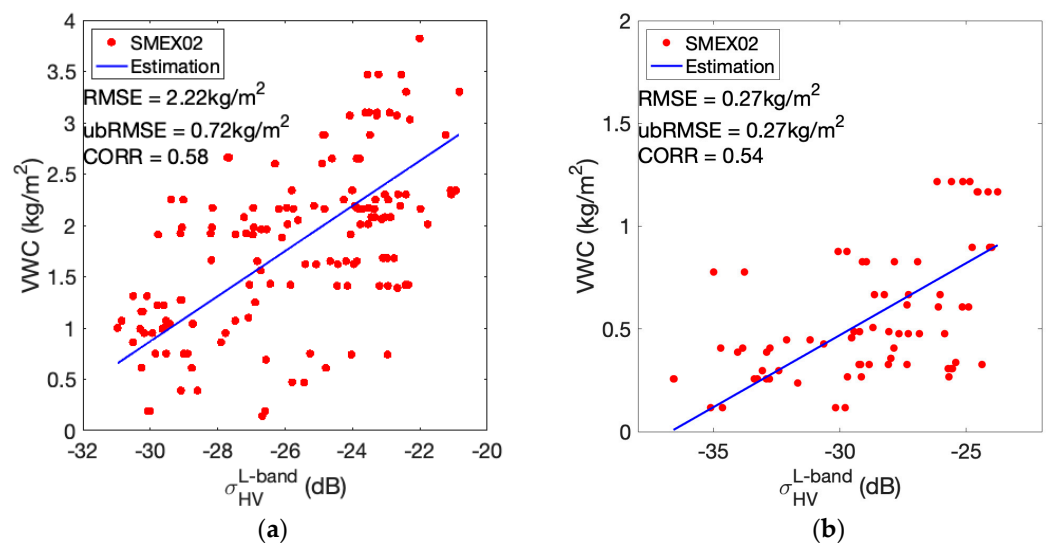


Figure 4. Comparison of NDWI derived VWC of SMEX02 (red dots, reference) and the estimated VWC (blue line) derived using the SMEX02 L-band HV and the SMAPVEX12 regression coefficients, Equations (1) and (2): (a) corn (b) soybean.

To assess the fidelity of the reference (NDWI-VWC), on the days when the in situ VWC is available, the two were compared. To fill the dates when in situ VWC values from destructive sampling were unavailable while both σ^0 and M_v were observed, we used VWC derived from the normalized difference water index (NDWI) [26]. For SMEX02 VWC was interpolated for each day using NDWI images obtained on different days [37]. Table 2 presented one site each for corn and soybean to show the comparison between in situ VWC and VWC derived from NDWI. We observed that in situ VWC only had two to four states, mostly two for all sites, while NDWI-derived VWC showed a gradual increase over this period. We knew the deficiency of in situ VWC could not fill all 8 flight days. We rather used NDWI derived VWC because it can both capture the growth of the crop during this period and the dynamic range is close to in situ VWCs.

Table 2. Comparison of VWC derived from NDWI and VWC sampled from in situ during flight period. The label flight (F) stands for days the radar measurements were taken. The label sampling (S) stands for days when VWC samplings were taken in fields.

(a) corn field 6									
Date	6/25	6/27	7/1	7/2	7/3	7/5	7/6	7/7	7/8
Flight/Sapling	F	F/S	F	F	S	F	F	F/S	F
VWC NDWI	2.71	3.17	3.99	4.11	NA	4.51	4.62	4.72	4.82
VWC in situ *	NA	3.17	NA	NA	4.7	NA	NA	5.57	NA
(b) soybean field 10									
Date	6/25	6/27	6/29	7/1	7/2	7/5	7/6	7/7	7/8
Flight/Sampling	F	F	S	F	F/S	F	F	F/S	F
VWC NDWI	0.35	0.44	NA	0.63	0.67	0.83	0.88	0.94	0.98
VWC in situ *	NA	NA	0.47	NA	0.49	NA	NA	1.19	NA

* Average is taken from sampling of 3 locations in this field.

For the soybean field, the unbiased RMSE of the HV-VWC is 0.28 kg/m² after removing the bias of 0.42 kg/m². For corn fields, the unbiased RMSE is 0.72 kg/m² after removing the bias of 2.22 kg/m².

4.2. Forward Model Validation

To validate the forward model fidelity, the backscattering coefficients were calculated using the L-band HV-derived VWC, and in situ data from soil moisture and soil rms height, they were compared with the SMEX02 radar observations.

First, for corn fields, Table 3 lists the error statistics of HH backscattering coefficients comparison at L- and S-band, L-HH and S-HH. For L-HH, the RMSE is large at an average of 3.32 dB and the averaged unbiased RMSE is reduced to 1.24 dB with an average correlation of 0.97. As an example, in field 6 shown in Figure 5a, the RMSE is 4.05 dB and the unbiased RMSE is 0.59 dB. The HV-derived VWC provides a reasonable level of unbiased RMSE in HH and will be consistently used in the retrieval. In a previous corn paper for SMAPVEX12 [16], the RMSE is 1.46 dB with a bias of 0.25 dB, meaning the unbiased RMSE is about 1.44 dB. The soil moisture retrieval was conducted well for SMAPVEX12. It is reasonable to justify that a ubRMSE of 1.24 dB for L-HH from Table 3 is good enough to consider the soil moisture retrieval.

Table 3. Forward Model Comparison of Backscattering at 21 Corn Fields; Within parenthesis are ubRMSE, RMSE, and correlation.

Site	L-HH	S-HH
1	(1.28, 4.22, 1.00)	(1.45, 1.77, 0.99)
4	(1.54, 4.34, 0.98)	(0.78, 0.99, 1.00)
5	(2.02, 2.19, 1.00)	(0.99, 2.16, 0.99)
6	(0.59, 4.05, 0.99)	(0.51, 1.19, 0.98)
8	(0.50, 1.25, 0.98)	(1.01, 2.01, 0.96)
11	(1.20, 3.78, 1.00)	(1.38, 2.17, 1.00)
12	(0.48, 2.23, 0.99)	(1.34, 2.60, 0.99)
15	(0.53, 3.97, 0.99)	(0.85, 1.32, 0.98)
17	(0.90, 2.19, 0.97)	(0.76, 1.21, 0.92)
18	(0.63, 3.43, 0.97)	(0.72, 1.94, 0.90)
19	(1.96, 2.98, 0.95)	(0.86, 1.22, 0.98)
20	(1.20, 2.89, 0.92)	(0.69, 0.89, 0.91)
24	(0.79, 3.53, 0.98)	(1.10, 1.29, 0.95)
25	(1.34, 3.41, 0.95)	(1.15, 1.17, 0.93)
26	(1.49, 1.77, 0.95)	(0.85, 1.70, 0.95)
27	(1.56, 6.31, 0.97)	(1.55, 1.59, 0.95)
28	(2.63, 3.07, 0.95)	(0.76, 2.06, 0.96)
30	(0.78, 5.12, 1.00)	(0.30, 0.70, 1.00)
33	(2.09, 2.50, 0.94)	(1.03, 1.79, 0.96)
Average	(1.24, 3.32, 0.97)	(0.95, 1.57, 0.96)

Site 29 and 31 are excluded because only 2 data points for the statistics. They are also excluded in the retrieval analysis. Data points with in situ VWC larger than 5 kg/m² were excluded, 13 out of 168 data points, because datacube's VWC range is within 5kg/m². Unit of ubRMSE and RMSE for VV and HH: dB.

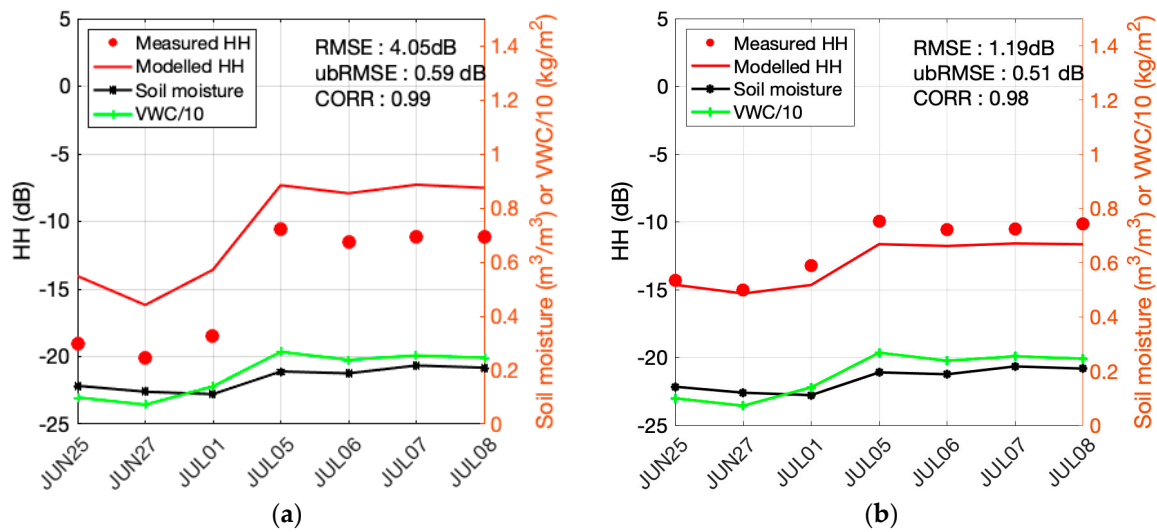


Figure 5. Forward model comparison of corn field at site 6 with rms height equal to 0.92cm (a) L-HH (b) S-HH.

At the S-band, the forward model simulates the observations well with the smaller unbiased RMSE than at L-band. Figure 5b shows the validation of S-HH at cornfield 6. The dynamic range of measured HH is about 5 dB compared with L-HH's 10 dB. The model correctly reflects the reduction in the dynamic range from the L- to S-band. The change in the dynamic range is most likely due to the penetration of radar signals. The L-band waves penetrate deeper through the vegetation layer and are able to detect both the temporal changes of VWC and soil moisture in Figure 5. Although it is usually considered the penetration is less as the frequency goes higher, the large dynamic range at the S-band shows that it is still possible to have a strong relationship between soil moisture and HH.

Second, for soybean fields, there are 10 fields from SMEX02. The unbiased RMSE is 0.99 dB at the L-band and 1.39 dB at the S-band (Table 4). Similar to corn's case, at both frequencies the forward model is reliable in terms of unbiased RMSE and correlation.

Table 4. Forward model comparison of backscattering coefficients for soybean. Within parenthesis are ubRMSE in dB, RMSE in dB, and correlation.

Site	L-HH	S-HH
3	(0.59, 0.89, 0.99)	(1.09, 2.31, 0.97)
9	(0.72, 1.18, 0.97)	(1.55, 1.94, 0.98)
10	(0.78, 1.16, 1.00)	(1.58, 2.02, 0.96)
13	(1.31, 1.46, 0.93)	(0.85, 1.76, 0.98)
14	(0.82, 1.77, 0.99)	(1.04, 1.32, 0.99)
16	(0.98, 4.22, 0.99)	(1.56, 1.93, 0.98)
21	(1.23, 1.84, 0.93)	(1.62, 1.66, 0.99)
22	(0.54, 2.04, 0.99)	(1.50, 2.63, 1.00)
23	(0.75, 0.78, 1.00)	(1.17, 1.52, 0.99)
32	(2.13, 4.58, 0.94)	(1.95, 2.19, 0.19)
Average	(0.99, 1.99, 0.97)	(1.39, 1.93, 0.90)

Figure 6 shows a time-series comparison of L-HH and S-HH at soybean field 10. The modeled HH has some bias possibly due to the choice of VWC_{adjust} , but the correlation shows that it follows the measurement well. As a result, the unbiased RMSE is reduced especially at the L-band. The measured L-HH in Figure 6a shows comparable overall dynamics, about 7 dB, as that from S-HH in Figure 6b. This is different from Figure 5 for corn where S-HH shows a reduced dynamic range. This can be explained by the penetration going deeper through the vegetation cover with soybean (smaller plant) than

with corn (larger plant). This should allow the soil moisture to influence the backscattering coefficients comparably at both the L- and S-band.

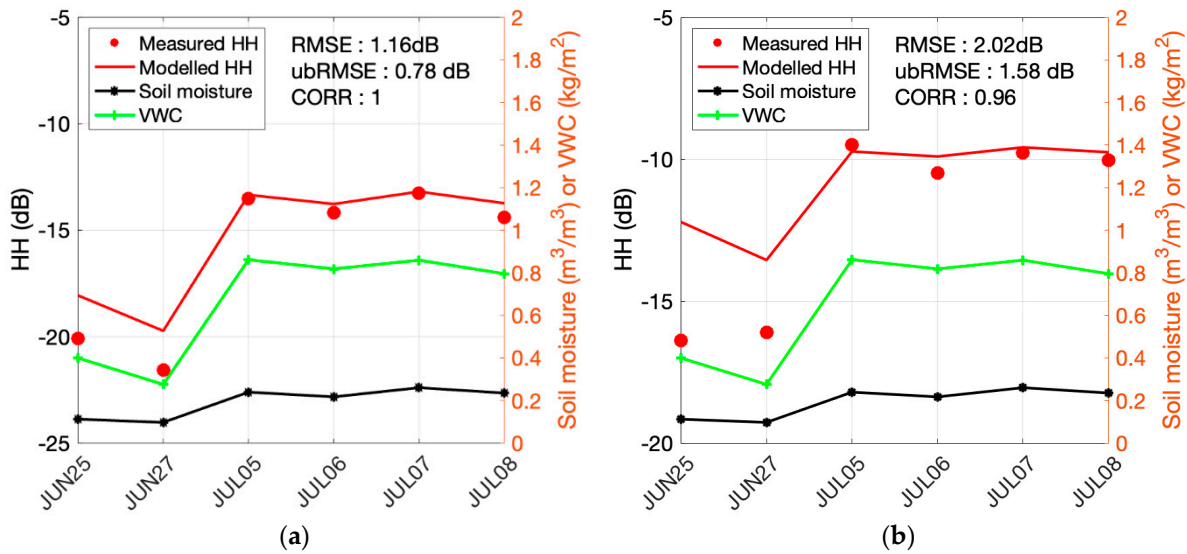


Figure 6. Forward model comparison of soybean field at site 10 (rms height: 1.08 cm) (a) L-HH (b) S-HH.

4.3. Soil Moisture Retrieval: Corn

Retrievals over corn fields show that the unbiased RMSE averaged over all the fields shows $0.041 \text{ m}^3/\text{m}^3$ and $0.39 \text{ m}^3/\text{m}^3$ with single frequency inputs L-HH and S-HH, respectively (Table 5). The retrieval performs well and the accuracy is comparable between the L-band and the S-band. As explained in Section 3.3, the single-frequency retrievals are slightly ill-conditions. To prevent the ill-condition during the time-series inversion, the retrieval from one time step to the next, the change in the retrieved dielectric constant is limited to 15% of the full dynamic range at each field. The full dynamic range is defined by the residual and saturated soil-moisture values determined by soil texture. Although the sensitivity of the S-band σ^0 to soil moisture in the vegetation presence is expected to be not as strong as in the L-band, the retrievals show that the dependence on soil moisture is strong, which is consistent with the forward model evaluation at the S-band.

Table 5. Soil moisture retrieval (Mv) validation of corn fields; within parenthesis are ubRMSE in m^3/m^3 , RMSE in m^3/m^3 and correlations.

Site	M_v^L	M_v^S	$M_v^{L\&S}$
1	(0.037, 0.063, 0.09)	(0.020, 0.033, 0.75)	(0.026, 0.047, 0.44)
4	(0.030, 0.041, 0.42)	(0.046, 0.064, 0.45)	(0.030, 0.047, 0.52)
5	(0.026, 0.059, 0.76)	(0.026, 0.059, 0.76)	(0.026, 0.059, 0.76)
6	(0.030, 0.031, 0.77)	(0.023, 0.055, 0.88)	(0.017, 0.028, 0.91)
8	(0.038, 0.038, 0.59)	(0.048, 0.053, 0.09)	(0.025, 0.029, 0.67)
11	(0.031, 0.031, 0.82)	(0.039, 0.039, 0.77)	(0.034, 0.034, 0.80)
12	(0.061, 0.071, -0.56)	(0.013, 0.079, 0.95)	(0.025, 0.033, 0.05)
15	(0.049, 0.050, -0.07)	(0.035, 0.068, 0.55)	(0.031, 0.039, 0.43)
17	(0.022, 0.083, 0.79)	(0.037, 0.102, 0.03)	(0.023, 0.091, 0.57)
18	(0.053, 0.054, 0.27)	(0.062, 0.165, -0.32)	(0.024, 0.074, -0.08)
19	(0.031, 0.082, 0.79)	(0.034, 0.078, 0.33)	(0.021, 0.076, 0.79)
20	(0.033, 0.066, 0.85)	(0.043, 0.069, 0.65)	(0.029, 0.063, 0.85)
24	(0.045, 0.047, 0.61)	(0.035, 0.093, 0.84)	(0.031, 0.059, 0.82)
25	(0.040, 0.049, 0.58)	(0.037, 0.102, 0.67)	(0.032, 0.069, 0.70)
26	(0.028, 0.060, 0.64)	(0.038, 0.076, -0.10)	(0.027, 0.066, 0.38)
27	(0.072, 0.088, 0.13)	(0.047, 0.050, 0.64)	(0.055, 0.058, 0.42)
28	(0.070, 0.079, 0.63)	(0.072, 0.160, 0.65)	(0.064, 0.083, 0.83)
30	(0.049, 0.049, -0.52)	(0.019, 0.060, 0.95)	(0.023, 0.036, 0.32)
33	(0.035, 0.092, 0.70)	(0.067, 0.230, 0.26)	(0.043, 0.158, 0.51)
Average	(0.041, 0.060, 0.44)	(0.039, 0.086, 0.52)	(0.031, 0.060, 0.56)

The retrieval in Table 5 shows that the L-band and L and S band have comparable average RMSEs of $0.06 \text{ m}^3/\text{m}^3$ while the S-band shows a larger RMSE of $0.086 \text{ m}^3/\text{m}^3$. We observe that the bias in the retrieval fluctuates from site to site (Table 5), while ubRMSE is fairly uniform from site to site. This observation underscores that ubRMSE is more representative of the retrieval accuracy from a statistical confidence viewpoint than RMSE would do. The unbiased RMSE from L- and S-band are $0.041 \text{ m}^3/\text{m}^3$ and $0.039 \text{ m}^3/\text{m}^3$, respectively. The dual-frequency retrievals produce the averaged unbiased RMSE of $0.031 \text{ m}^3/\text{m}^3$, smaller than either L- or S-band single-channel retrievals. By averaging the retrieved soil moisture from both frequencies, more accurate retrievals were achieved than from single frequency input. The merit of the averaging in soil moisture space was discussed in detail in Section 3.4. The averaging of the results from the L- and S-bands reduces the ill-condition to achieve better soil moisture retrieval.

Figure 7 compares the single- and dual-frequency retrieval in one field. The dual-frequency retrieval shows better unbiased RMSE for this site, $0.017 \text{ m}^3/\text{m}^3$, than single-frequency estimates because of the compensation of slightly underestimated and overestimated soil moisture from the L- and S-bands, respectively.

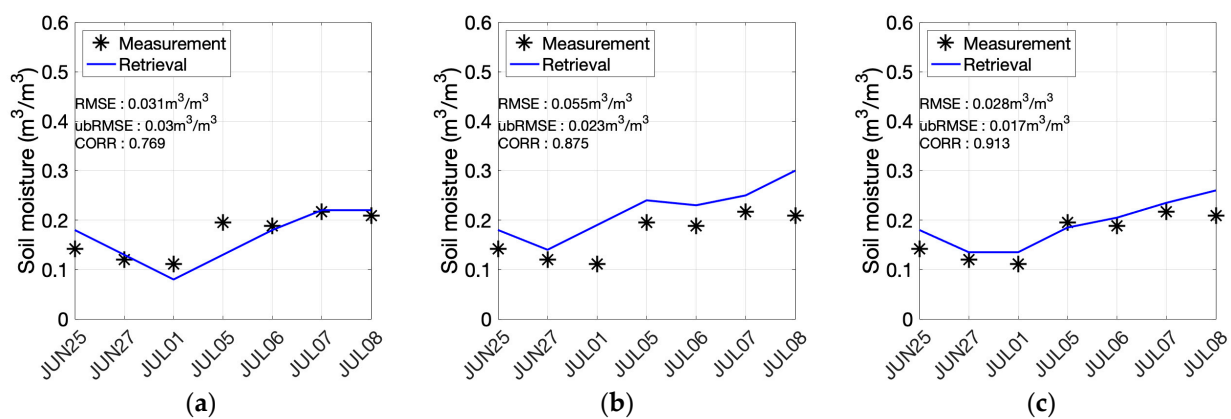


Figure 7. Soil moisture retrieval at corn site 6 from (a) L-band (b) S-band (c) combined L- and S-band.

4.4. Soil Moisture Retrieval: Soybean

Retrievals over soybean fields show that the unbiased RMSE averaged over all the fields shows $0.059 \text{ m}^3/\text{m}^3$ and $0.061 \text{ m}^3/\text{m}^3$ with single frequency inputs L-HH and S-HH, respectively (Table 6). The retrieval accuracy is comparable between the L-band and the S-band. We apply the same constraint to the retrieval for soybean fields as in the corn case. The retrieval in Table 6 shows average RMSEs of about $0.074 \text{ m}^3/\text{m}^3$ or more. After the removal of the bias, the average unbiased RMSE from L- and S-band are $0.059 \text{ m}^3/\text{m}^3$ and $0.061 \text{ m}^3/\text{m}^3$, respectively. The dual-frequency retrievals produce the averaged unbiased RMSE of $0.057 \text{ m}^3/\text{m}^3$, slightly better than either the L- or S-band single channel retrievals. The averaging of the results from the L- and S-bands again reduces the ill-condition to achieve better soil moisture retrieval.

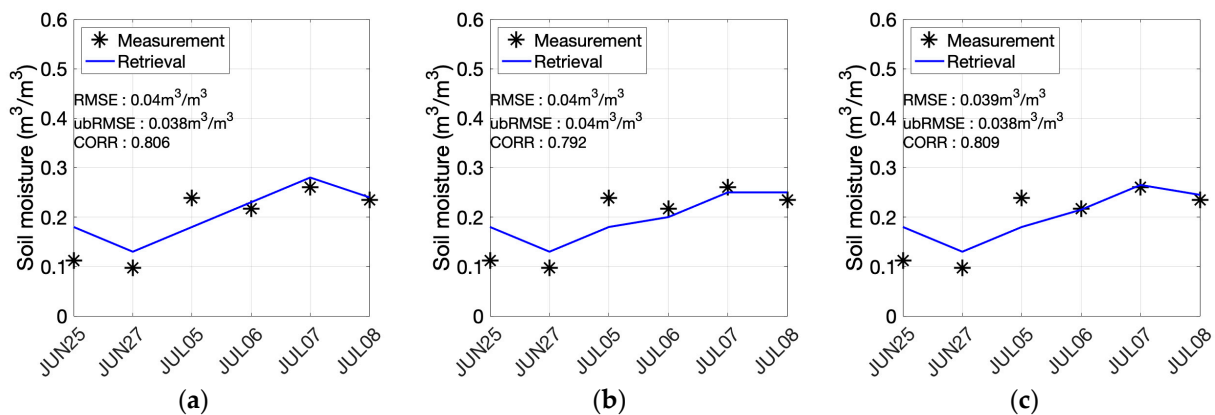
Overall, the retrieval error over soybean fields is about $0.02 \text{ m}^3/\text{m}^3$ higher than the performance over corn fields. We observe in the forward matching from Figure 6 that the HH backscatters at the first two dates with low VWC are over-estimated compared to the rest of the dates in the time series. This may be improved by applying the coherent model for an early stage of soybean with low VWC [15]. From [15], for VWC lower than $0.2 \text{ kg}/\text{m}^2$, the incoherent model over-estimates the backscattering by 2~3 dB compared to the coherent models. The coherent model adds the scattered waves in complex numbers (that is, the phase of the electromagnetic waves is considered during the addition). When scatterers are close to each other as in the young soybean (indicated by low VWC), such addition reduces the total backscattering from multiple scatterers.

Table 6. Soil moisture retrieval validation at soybean fields; Within parenthesis are unbiased RMSE in m^3/m^3 , RMSE in m^3/m^3 and correlation.

Site	M_v^L	M_v^S	$M_v^{L\&S}$
3	(0.038, 0.059, 0.86)	(0.074, 0.116, −0.39)	(0.037, 0.043, 0.79)
9	(0.071, 0.071, −0.54)	(0.061, 0.086, −0.06)	(0.062, 0.071, −0.37)
10	(0.038, 0.040, 0.81)	(0.040, 0.040, 0.79)	(0.038, 0.039, 0.81)
13	(0.053, 0.061, −0.42)	(0.037, 0.074, 0.37)	(0.047, 0.067, −0.31)
14	(0.046, 0.047, 0.51)	(0.075, 0.080, −0.39)	(0.060, 0.061, 0.04)
16	(0.099, 0.116, −0.74)	(0.074, 0.081, −0.39)	(0.086, 0.098, −0.63)
21	(0.025, 0.048, 0.68)	(0.036, 0.046, 0.39)	(0.029, 0.045, 0.55)
22	(0.081, 0.084, −0.28)	(0.098, 0.107, −0.47)	(0.089, 0.095, −0.39)
23	(0.053, 0.063, 0.62)	(0.059, 0.059, 0.48)	(0.055, 0.057, 0.59)
32	(0.090, 0.233, −0.34)	(0.051, 0.105, 0.14)	(0.069, 0.168, −0.17)
Average	(0.059, 0.082, 0.12)	(0.061, 0.079, 0.05)	(0.057, 0.074, 0.09)

Examining the retrievals for the two crops together, we observe that the L-band retrieval does not show significantly better performance than the S-band. Often, it is expected that the sensitivity between backscatter and soil moisture improves with longer wavelengths because the penetration through vegetation improves. Our results show that the penetration may not be significantly reduced, which allows the model to retrain similar retrieval performance among L- and S-bands.

Figure 8 shows the retrieved soil moisture in time sequence from the L-, S-, and combined L- and S-band. Either method shows a good correlation between the measured and the retrieved soil moisture.

**Figure 8.** Soil moisture retrieval at soybean site 10 from (a) L-band (b) S-band (c) combined L- and S-bands.

5. Discussion

5.1. Comparison of Retrievals Using Single Band and Two Bands

The single-frequency retrieval of soil moisture is found effective in this study for both corn and soybean. In the literature, S-band retrievals are rare. Narayan et al. made various combinations of brightness temperature and radar backscatters observed at L- and S-bands from the SMEX02 campaign to perform regression-based soil moisture retrievals [22]. However, they did not use S-HH or single-frequency retrieval. In the current study, the S-HH-only retrieval provides satisfactory results. This result implies that both the L- and S-band have significant sensitivity to soil moisture change on their own. Based on this finding, we combine L- and S-bands by averaging the retrieved soil moisture. By averaging the retrieved soil moisture from both frequencies, we further improve the retrieval performance. This avoids the determination (that is uncertain) of the weights of L- and S-bands σ_0 if the σ_0 minimization is formulated together in one cost function during the soil moisture retrieval.

5.2. Retrieval Sensitivity against VWC Bias

In the retrieval, VWC was first estimated using Equations (1) and (2). The regression between the reference VWC and L-band HV was from the SMAPVEX12 campaign. However, we introduced the term VWC_{adjust} to ensure all estimated VWCs are non-negative. The correlation is high as shown in Figure 4. We used a VWC_{adjust} of 1 kg/m² and 0.06 kg/m² for corn and soybean, respectively. However, VWC_{adjust} was manually assigned to have a better agreement in Figure 4. Here, we show the sensitivity test of retrieval performance against VWC_{adjust} for both crops. By varying VWC_{adjust} , we repeated the calculation of the soil moisture retrieval at the L-band and S-band. We then calculated the average soil moisture. These steps were repeated for different VWC_{adjust} values. The statistics error was then calculated and listed in Tables 7 and 8 for corn and soybean. In Table 7, we varied VWC_{adjust} from 1 to 1.4 kg/m², about 6% of the overall dynamic range of 6.5 kg/m². The unbiased RMSE did not fluctuate significantly for all three columns, within 0.006 m³/m³. Moreover, all of them showed that average soil moisture from the L- and S-bands performed the best. For the soybean in Table 8, we varied VWC_{adjust} from 0.06 to 0.14 kg/m², about 6% of the overall dynamic range of 1.3 kg/m². Soybean also showed no significant sensitivity against the choice of VWC_{adjust} . We also found that VWC_{adjust} has no sensitivity to RMSE.

Table 7. Sensitivity test of soil moisture retrieval validation at corn fields for different VWC_{adjust} ; Within parenthesis are unbiased RMSE in m³/m³, RMSE in m³/m³ and correlation.

VWC_{adjust}	M_v^L	M_v^S	$M_v^{L\&S}$
1	(0.041, 0.060, 0.44)	(0.039, 0.086, 0.52)	(0.031, 0.060, 0.56)
1.1	(0.038, 0.057, 0.54)	(0.036, 0.076, 0.59)	(0.030, 0.059, 0.69)
1.2	(0.040, 0.059, 0.54)	(0.034, 0.079, 0.64)	(0.031, 0.061, 0.70)
1.3	(0.039, 0.060, 0.60)	(0.036, 0.066, 0.66)	(0.033, 0.058, 0.71)
1.4	(0.040, 0.061, 0.63)	(0.039, 0.059, 0.62)	(0.036, 0.057, 0.68)

Table 8. Sensitivity test of soil moisture retrieval validation at soybean fields for different VWC_{adjust} ; Within parenthesis are unbiased RMSE in m³/m³, RMSE in m³/m³ and correlation.

VWC_{adjust}	M_v^L	M_v^S	$M_v^{L\&S}$
0.06	(0.059, 0.082, 0.12)	(0.061, 0.079, 0.05)	(0.057, 0.074, 0.09)
0.08	(0.061, 0.080, 0.08)	(0.062, 0.079, 0.02)	(0.060, 0.076, 0.06)
0.10	(0.060, 0.080, 0.10)	(0.061, 0.079, 0.03)	(0.060, 0.077, 0.07)
0.12	(0.060, 0.083, 0.09)	(0.057, 0.074, 0.16)	(0.057, 0.076, 0.14)
0.14	(0.060, 0.083, 0.12)	(0.058, 0.076, 0.16)	(0.057, 0.076, 0.16)

The choice of VWC_{adjust} did not alter the slope between VWC and L-band HV, Equations (1) and (2). The model captured the trend of VWC over time. Although there could be bias due to the choice of VWC_{adjust} , it did not create a significant difference in the retrieval from the sensitivity test in Table 7. This also suggests that we may extend the regression formulas in Equations (1) and (2) to other independent locations with the same crops. Although we will need to have other VWC_{adjust} values, the choice may be more flexible because of the insensitivity to alter the retrieval.

The bias in the VWC estimate was removed empirically in this study. Alternatively, such bias can be estimated as a part of the retrieval, as formulated and demonstrated in [14]. In this scheme, the cost function optimizes both soil moisture and VWC bias. This additional unknown may deteriorate the soil moisture retrieval due to the additional unknown or, conversely, may improve. This issue will be investigated in future work. Instead, in this paper, we focused on using L-HH and S-HH to demonstrate the improvement of soil moisture retrieval from single frequency to dual frequencies.

6. Conclusions

In this paper, with the coming NISAR mission featuring two frequencies, L- and S-bands, we evaluate the soil moisture retrieval performance using these two frequencies. The key accomplishments in this paper include:

1. The physical model for the radar forward scattering established in the SMAPVEX12 campaign for just the L-band is now successfully extended to S-band. The two frequencies are close enough to each other for the vegetation modeling to remain the same. The model is independently validated with the data from the separate field campaign, SMEX02, for corn and soybean fields.
2. The retrieval algorithm using the time-series input backscatter works well. The dual-frequency L-HH and S-HH input gives a soil moisture retrieval with an unbiased RMSE that is better than the single frequencies for both corn and soybean. The unbiased RMSE for corn is $0.031 \text{ m}^3/\text{m}^3$ and the unbiased RMSE for soybean is $0.057 \text{ m}^3/\text{m}^3$. There are two findings from the results. First, either L- or S-band single-frequency retrieval has sensitivity and reliable performance for soil moisture retrieval, even if each retrieval is slightly underdetermined. Second, averaging the retrieved soil moisture from both frequencies, further improves the retrieval performance. This avoids the determination (that is uncertain) of the weights of L- and S-bands σ_0 if the σ_0 minimization is formulated together in one cost function during the soil moisture retrieval.
3. The in this study is estimated with HV polarization at the L-band separately for both corn and soybean. The empirical relationships between HV and VWC established from the SMAPVEX12 campaign apply well to estimate for VWC for SMEX02. The regression equation is applied with adjustable VWC bias. It is shown that the retrieval performance is not sensitive to VWC bias. This supports the prospect that the empirical relationship may apply to wider regions of the same crop type. To apply this HV-VWC globally, the VWC bias can be estimated by comparing it with daily climatology data. The NASA SMAP mission produced a 1 km VWC daily climatology database [38]. This will be expanded by the upcoming NISAR mission to generate a 200 m daily climatology database.

Author Contributions: Both authors devised the study. The simulation and validation were conducted by T.-H.L.; The data processing, generation and analysis of results were performed by T.-H.L. and S.-B.K.; T.-H.L. generated the figures and the draft. Both authors contributed to writing and revising the manuscript. All authors have read and agreed to the published version of the manuscript.

Funding: The portion of this research was carried out at the Jet Propulsion Laboratory, California Institute of Technology, under a contract with the National Aeronautics and Space Administration (80NM0018D0004).

Conflicts of Interest: The authors declare no conflict of interest.

References

1. Bauer-Marschallinger, B.; Freeman, V.; Cao, S.; Paulik, C.; Schauffer, S.; Stachl, T.; Modanesi, S.; Massari, C.; Ciabatta, L.; Brocca, L.; et al. Toward Global Soil Moisture Monitoring With Sentinel-1: Harnessing Assets and Overcoming Obstacles. *IEEE Trans. Geosci. Remote Sens.* **2019**, *57*, 520–539. [[CrossRef](#)]
2. Entekhabi, D.; Njoku, E.G.; O'Neill, P.E.; Kellogg, K.H.; Crow, W.T.; Edelstein, W.N.; Entin, J.K.; Goodman, S.D.; Jackson, T.J.; Johnson, J.; et al. The Soil Moisture Active Passive (SMAP) Mission. *Proc. IEEE* **2010**, *98*, 704–716. [[CrossRef](#)]
3. Kim, S.-B.; Zyl, J.J.; van Johnson, J.T.; Moghaddam, M.; Tsang, L.; Colliander, A.; Dunbar, R.S.; Jackson, T.J.; Jaruwatanadilok, S.; West, R.; et al. Surface Soil Moisture Retrieval Using the L-Band Synthetic Aperture Radar Onboard the Soil Moisture Active–Passive Satellite and Evaluation at Core Validation Sites. *IEEE Trans. Geosci. Remote Sens.* **2017**, *55*, 1897–1914. [[CrossRef](#)] [[PubMed](#)]
4. Kellogg, K.; Hoffman, P.; Standley, S.; Shaffer, S.; Rosen, P.; Edelstein, W.; Dunn, C.; Baker, C.; Barela, P.; Shen, Y.; et al. NASA-ISRO Synthetic Aperture Radar (NISAR) Mission. In Proceedings of the 2020 IEEE Aerospace Conference, Big Sky, MT, USA, 7–14 March 2020; pp. 1–21.

5. Stavros, N.; Siqueira, P.; Cosh, M.; Torbick, N.; Osmanoglu, B. *2018 NISAR Applications Workshop: Agriculture and Soil Moisture*; Jet Propulsion Laboratory California Institute of Technology: Pasadena, CA, USA, 2019; 36p.
6. Ouellette, J.D.; Johnson, J.T.; Balenzano, A.; Mattia, F.; Satalino, G.; Kim, S.-B.; Dunbar, R.S.; Colliander, A.; Cosh, M.H.; Caldwell, T.G.; et al. A Time-Series Approach to Estimating Soil Moisture From Vegetated Surfaces Using L-Band Radar Backscatter. *IEEE Trans. Geosci. Remote Sens.* **2017**, *55*, 3186–3193. [[CrossRef](#)]
7. Jagdhuber, T.; Hajnsek, I.; Papathanassiou, K.P. An Iterative Generalized Hybrid Decomposition for Soil Moisture Retrieval Under Vegetation Cover Using Fully Polarimetric SAR. *IEEE J. Sel. Top. Appl. Earth Obs. Remote Sens.* **2015**, *8*, 3911–3922. [[CrossRef](#)]
8. Tabatabaenejad, A.; Burgin, M.; Moghaddam, M. Potential of L-Band Radar for Retrieval of Canopy and Subcanopy Parameters of Boreal Forests. *IEEE Trans. Geosci. Remote Sens.* **2012**, *50*, 2150–2160. [[CrossRef](#)]
9. Bousbih, S.; Zribi, M.; Lili-Chabaane, Z.; Baghdadi, N.; El Hajj, M.; Gao, Q.; Mougenot, B. Potential of Sentinel-1 Radar Data for the Assessment of Soil and Cereal Cover Parameters. *Sensors* **2017**, *17*, 2617. [[CrossRef](#)] [[PubMed](#)]
10. Paloscia, S.; Pettinato, S.; Santi, E.; Notarnicola, C.; Pasolli, L.; Reppucci, A. Soil Moisture Mapping Using Sentinel-1 Images: Algorithm and Preliminary Validation. *Remote Sens. Environ.* **2013**, *134*, 234–248. [[CrossRef](#)]
11. Wang, H.; Magagi, R.; Goita, K.; Wang, K. Soil Moisture Retrievals Using ALOS2-ScanSAR and MODIS Synergy over Tibetan Plateau. *Remote Sens. Environ.* **2020**, *251*, 112100. [[CrossRef](#)]
12. Pierdicca, N.; Pulvirenti, L.; Pace, G. A Prototype Software Package to Retrieve Soil Moisture From Sentinel-1 Data by Using a Bayesian Multitemporal Algorithm. *IEEE J. Sel. Top. Appl. Earth Obs. Remote Sens.* **2014**, *7*, 153–166. [[CrossRef](#)]
13. Kim, S.-B.; Tsang, L.; Johnson, J.T.; Huang, S.; van Zyl, J.J.; Njoku, E.G. Soil Moisture Retrieval Using Time-Series Radar Observations Over Bare Surfaces. *IEEE Trans. Geosci. Remote Sens.* **2012**, *50*, 1853–1863. [[CrossRef](#)]
14. Kim, S.-B.; Moghaddam, M.; Tsang, L.; Burgin, M.; Xu, X.; Njoku, E.G. Models of L-Band Radar Backscattering Coefficients Over Global Terrain for Soil Moisture Retrieval. *IEEE Trans. Geosci. Remote Sens.* **2014**, *52*, 1381–1396. [[CrossRef](#)]
15. Huang, H.; Kim, S.-B.; Tsang, L.; Xu, X.; Liao, T.-H.; Jackson, T.J.; Yueh, S.H. Coherent Model of L-Band Radar Scattering by Soybean Plants: Model Development, Evaluation, and Retrieval. *IEEE J. Sel. Top. Appl. Earth Obs. Remote Sens.* **2016**, *9*, 272–284. [[CrossRef](#)]
16. Liao, T.-H.; Kim, S.-B.; Tan, S.; Tsang, L.; Su, C.; Jackson, T.J. Multiple Scattering Effects With Cyclical Correction in Active Remote Sensing of Vegetated Surface Using Vector Radiative Transfer Theory. *IEEE J. Sel. Top. Appl. Earth Obs. Remote Sens.* **2016**, *9*, 1414–1429. [[CrossRef](#)]
17. Huang, H.; Liao, T.-H.; Kim, S.B.; Xu, X.; Tsang, L.; Jackson, T.J.; Yueh, S.H. L-Band Radar Scattering and Soil Moisture Retrieval of Wheat, Canola and Pasture Fields for Snap Active Algorithms. *Prog. Electromagn. Res.* **2021**, *170*, 129–152. [[CrossRef](#)]
18. Kurum, M.; Kim, S.-B.; Akbar, R.; Cosh, M.H. Surface Soil Moisture Retrievals Under Forest Canopy for L-Band SAR Observations Across a Wide Range of Incidence Angles by Inverting a Physical Scattering Model. *IEEE J. Sel. Top. Appl. Earth Obs. Remote Sens.* **2021**, *14*, 1741–1753. [[CrossRef](#)]
19. Akbar, R.; Moghaddam, M. A Combined Active–Passive Soil Moisture Estimation Algorithm With Adaptive Regularization in Support of SMAP. *IEEE Trans. Geosci. Remote Sens.* **2015**, *53*, 3312–3324. [[CrossRef](#)]
20. Jackson, T.; Cosh, M. SMEX02 Watershed Soil Moisture Data, Walnut Creek, Iowa, Version 1. Available online: <https://nsidc.org/data/nsidc-0143/versions/1> (accessed on 11 August 2022).
21. Bolten, J.D.; Lakshmi, V.; Njoku, E.G. Soil Moisture Retrieval Using the Passive/Active L- and S-Band Radar/Radiometer. *IEEE Trans. Geosci. Remote Sens.* **2003**, *41*, 2792–2801. [[CrossRef](#)]
22. Narayan, U. Retrieval of Soil Moisture from Passive and Active L/S Band Sensor (PALS) Observations during the Soil Moisture Experiment in 2002 (SMEX02). *Remote Sens. Environ.* **2004**, *92*, 483–496. [[CrossRef](#)]
23. Kim, S.-B.; Liao, T.-H. Robust retrieval of soil moisture at field scale across wide-ranging SAR incidence angles for soybean, wheat, forage, oat and grass. *Remote Sens. Environ.* **2021**, *266*, 112712. [[CrossRef](#)]
24. Colliander, A.; Chan, S.; Kim, S.; Das, N.; Yueh, S.; Cosh, M.; Bindlish, R.; Jackson, T.; Njoku, E. Long Term Analysis of PALS Soil Moisture Campaign Measurements for Global Soil Moisture Algorithm Development. *Remote Sens. Environ.* **2012**, *121*, 309–322. [[CrossRef](#)]
25. Anderson, M. SMEX02 Regional Vegetation Sampling Data, Iowa, Version 1 [Data Set]. Boulder, Colorado USA. NASA National Snow and Ice Data Center Distributed Active Archive Center. 2003. Available online: <https://nsidc.org/data/nsidc-0188/versions/1> (accessed on 18 May 2018).
26. Jackson, T.J.; Chen, D.; Cosh, M.; Li, F.; Anderson, M.; Walthall, C.; Doriaswamy, P.; Hunt, E.R. Vegetation Water Content Mapping Using Landsat Data Derived Normalized Difference Water Index for Corn and Soybeans. *Remote Sens. Environ.* **2004**, *92*, 475–482. [[CrossRef](#)]
27. Lang, R.H.; Sighu, J.S. Electromagnetic Backscattering from a Layer of Vegetation: A Discrete Approach. *IEEE Trans. Geosci. Remote Sens.* **1983**, *GE-21*, 62–71. [[CrossRef](#)]
28. Tsang, L.; Kong, J.A.; Ding, K.-H. *Scattering of Electromagnetic Waves Vol. 1: Theories and Applications*; John Wiley & Sons, Inc.: New York, NY, USA, 2000. [[CrossRef](#)]
29. Ulaby, F.T.; Moore, R.K.; Fung, A.K. *Microwave Remote Sensing Active and Passive—Volume III: From Theory to Applications*; Artech House Inc: London, UK, 1986.
30. Ulaby, F.T.; El-rayes, M.A. Microwave Dielectric Spectrum of Vegetation—Part II: Dual-Dispersion Model. *IEEE Trans. Geosci. Remote Sens.* **1987**, *GE-25*, 550–557. [[CrossRef](#)]

31. Huang, S.; Tsang, L. Electromagnetic Scattering of Randomly Rough Soil Surfaces Based on Numerical Solutions of Maxwell Equations in Three-Dimensional Simulations Using a Hybrid UV/PBTG/SMCG Method. *IEEE Trans. Geosci. Remote Sens.* **2012**, *50*, 4025–4035. [[CrossRef](#)]
32. Wu, T.-D.; Chen, K.-S.; Shi, J.; Lee, H.-W.; Fung, A.K. A Study of an AIEM Model for Bistatic Scattering From Randomly Rough Surfaces. *IEEE Trans. Geosci. Remote Sens.* **2008**, *46*, 2584–2598. [[CrossRef](#)]
33. Kim, Y.; van Zyl, J.J. A Time-Series Approach to Estimate Soil Moisture Using Polarimetric Radar Data. *IEEE Trans. Geosci. Remote Sens.* **2009**, *47*, 2519–2527. [[CrossRef](#)]
34. Ma, J.; Huang, S.; Li, J.; Li, X.; Song, X.; Leng, P.; Sun, Y. Estimating Vegetation Water Content of Corn and Soybean Using Different Polarization Ratios Based on L- and S-Band Radar Data. *IEEE Geosci. Remote Sens. Lett.* **2017**, *14*, 364–368. [[CrossRef](#)]
35. Kim, S.; Van Zyl, J.; Dunbar, R.S.; Njoku, E.G.; Johnson, J.T.; Moghaddam, M.; Tsang, L. *SMAP L3 Radar Global Daily 3 Km EASE-Grid Soil Moisture, Version 3*; NASA National Snow and Ice Data Center Distributed Active Archive Center: Boulder, CO, USA, 2016.
36. Mironov, V.L.; Dobson, M.C.; Kaupp, V.H.; Komarov, S.A.; Kleshchenko, V.N. Generalized Refractive Mixing Dielectric Model for Moist Soils. *IEEE Trans. Geosci. Remote Sens.* **2004**, *42*, 773–785. [[CrossRef](#)]
37. Colliander, A.; Chan, S.; Yueh, S.; Cosh, M.; Bindlish, R.; Jackson, T.; Njoku, E. Utilization of airborne and in situ data obtained in SGP99, SMEX02, CLASIC and SMAPVEX08 Field Campaigns for SMAP Soil Moisture Algorithm Development and Validation. In Proceedings of the 2010 11th Specialist Meeting on Microwave Radiometry and Remote Sensing of the Environment, Washington, DC, USA, 1–4 March 2010; pp. 43–48. [[CrossRef](#)]
38. Available online: https://smap.jpl.nasa.gov/system/internal_resources/details/original/289_047_veg_water.pdf (accessed on 1 November 2022).